Journal of Solid State Chemistry **147,** 309–319 (1999)
Article ID jssc.1999.8287, available online at http://www.idealibrary.com on IDEAL®

Eightfold Superstructure in $K_2Gd_2Sb_2Se_9$ and $K_2La_2Sb_2S_9$ Caused by Three-Dimensional Ordering of the $5s^2$ Lone Pair of Sb^{3+} Ions

Kyoung-Shin Choi, Jason A. Hanko, and Mercouri G. Kanatzidis[1]

Department of Chemistry and Center for Fundamental Materials Research, Michigan State University, East Lansing, Michigan 48824

Received November 4, 1998; accepted March 23, 1999

DEDICATED TO PROFESSOR JEAN ROUXEL IN MEMORIAM

The new isostructural compounds, $K_2Gd_2Sb_2Se_9$ and $K_2La_2Sb_2S_9$, were discovered by the molten polychalcogenide salt method. They crystallize in the orthorhombic space group *Pbam* with $a = 11.4880(3)$ Å, $b = 17.6612(1)$ Å, $c = 4.2201(1)$ Å, and $Z = 2$ for $K_2Gd_2Sb_2Se_9$ and $a = 11.2080(5)$ Å, $b = 16.8781(8)$ Å, $c = 4.2419(2)$ Å, and $Z = 2$ for $K_2La_2Sb_2S_9$. The compounds have a three-dimensional $[M_2Sb_2Q_9]^{2-}$ framework (M = Gd, La; Q = Se, S) with K^+-ion-filled channels running along the c axis. The coordination geometry around the rare earth atom is best described as a bicapped trigonal prism. The Gd^{3+}/La^{3+} centered trigonal prisms share triangular faces with neighboring prisms forming one-dimensional columns along the c axis. The columns are connected to each other to form sheets by sharing Se/S atoms on the capping sites of the trigonal prisms. Sb^{3+} ions are stabilized in distorted octahedral sites. The SbQ_6 (Q = Se, S) octahedra share edges with neighboring octahedra making an infinite chain along the c axis and bridging Gd/La layers together to make the whole framework three-dimensional. In both compounds, Sb atoms appear to be positionally disordered over two crystallographically different sites with half occupancy. This disorder was removed upon elucidation of a $2a \times 2b \times 2c$ superstructure, which more accurately describes the positional ordering of Sb atoms in the structure. The superstructure of $K_2Gd_2Sb_2Se_9$ was refined in the monoclinic space group $C2/m$ with $a = 22.8783(4)$ Å, $b = 8.4062(2)$ Å, $c = 20.970(1)$ Å, $\beta = 123.022(1)^\circ$, and $Z = 8$. These compounds are semiconductors with band gap values of 1.33 eV for $K_2Gd_2Sb_2Se_9$ and 2.20 eV for $K_2La_2Sb_2S_9$. Magnetic susceptibility measurements indicate no apparent magnetic coupling between the Gd^{3+} centers showing Curie–Weiss behavior with $\mu_{eff} = 7.96$ B.M. $K_2Gd_2Sb_2Se_9$ melts congruently at 598°C while $K_2La_2Sb_2S_9$ decomposes gradually above 400°C. The Raman spectra show the diselenide stretching vibration in $K_2Gd_2Sb_2Se_9$ at 266 cm^{-1} and the disulfide stretching vibration in $K_2La_2Sb_2S_9$ at 473 cm^{-1}. © 1999 Academic Press

1. INTRODUCTION

To explore the solid state chemistry of multinary chalcoantimonate compounds, we have extended the alkali metal polychalcophosphate flux method (1) to the chalcoantimonate fluxes. These fluxes are formed by the *in situ* fusion of $A_2Q/Sb/Q$ or $A_2Q/Sb_2Q_3/Q$ (A = K, Rb, Cs; Q = S, Se) to produce various $A_x[Sb_yQ_z]$ units. These discrete species can vary in composition and structure and can form the basis for generating a large number of quaternary and ternary compounds in a rational and systematic way. Antimony compounds are expected to have structural diversity due to the tendency of the Sb 5*s* lone pair to adopt various stereochemical shapes. This tendency is generally more pronounced in the Sb compounds than in the corresponding Bi compounds. We have already reported the synthesis and characterization of several new multinary chalcoantimonates obtained from this method, such as $KThSb_2Se_6$ (2), $K_2Sb_8Se_{13}$ (3), $K_{2.5}Sb_{8.5}Se_{14}$ (3), A_2AgSbS_4 (A = K, Rb, Cs) (4), $Cs_3Ag_2Sb_3Q_8$ (Q = S, Se) (4), $Rb_2Au_6Sb_4S_{10}$ (5), A_2AuSbS_4 (A = Rb, Cs) (6), $A_2Ag_{20}Sb_4S_{19}$ (A = Rb, Cs) (7). Considering that the number of quaternary compounds in this class is limited (e.g., $KHgSbS_3$ (8), $RbHgSbTe_3$ (9), $K_2(RE)_{2-x}Sb_xSb_4Se_{12}$ (RE = La, Ce, Pr, Gd) (10)) and that the physicochemical characterization of most mineral sulfosalts is incomplete, additional studies on this type of compound with various elements and compositions will provide us with better understanding of solid state Sb chemistry. Work that includes rare earth and actinide metals is of particular interest because the very large *f* elements, along with the lone pair of Sb^{3+} ions, can induce interesting low symmetry structures with various kinds of distortion leading to unusual arrangements. For example, $KThSb_2Se_6$ and AU_2SbQ_8 (A = K, Rb; Q = S, Se) (11) show new structure types with a unique local environment for the actinide metals and antimony atoms. Here we report the synthesis and structural study of the new lanthanide chalcoantimonate compounds, $K_2Gd_2Sb_2Se_9$ and $K_2La_2Sb_2S_9$. The Sb^{3+}

[1] To whom correspondence should be addressed.

0022-4596/99 $30.00

atoms in these compounds sit on octahedral sites made by Se/S atoms. At first, the Sb^{3+} atoms appeared to be positionally disordered, within the same octahedron, over two different sites located 0.26 Å away from the center, reminiscent of a double potential well system of equal energy. However, this model does not represent the true picture in this structure and a closer look at the X-ray scattering properties of the materials revealed the presence of a $2a \times 2b \times 2c$ superstructure. This superstructure lifts the disorder among the Sb atoms and more accurately describes their distribution. Both the substructure and the superstructure were refined and their differences are discussed. The magnetic properties, thermal stability, and optical and Raman spectra for both compounds are reported.

2. EXPERIMENTAL

2.1. Synthesis

The following reagents were used as obtained: gadolinium, −40 mesh (Cerac, Milwaukee, WI); lanthanum, 40 mesh (Cerac, Milwaukee, WI); antimony, −200 mesh (Cerac, Milwaukee, WI); selenium powder, 100 mesh (Aldrich, Milwaukee, WI); sulfur powder, sublimed (JT Baker Co., Phillipsburg, NJ); and potassium metal, analytical reagent (Mallinckrodt, Inc., Paris, KY). The K_2Se/K_2S starting materials were prepared by a stoichiometric reaction of potassium metal and selenium/sulfur in liquid NH_3. Sb_2Se_3 was prepared by heating a stoichiometric mixture of antimony and selenium at 750°C for 48 h.

$K_2Gd_2Sb_2Se_9$. This compound was synthesized from a mixture of 0.0628 g (0.4 mmol) K_2Se, 0.0629 g (0.4 mmol) Gd, 0.0961 g (0.2 mmol) Sb_2Se_3, and 0.1579 g (2 mmol) Se. The reagents were thoroughly mixed, sealed in an evacuated Pyrex ampoule, and heated at 540°C for 5 days (cooling 2°C/h). Pure black needles of $K_2Gd_2Sb_2Se_9$ were obtained by isolation in degassed dimethylformamide (DMF) and water (yield >95% based on Gd metal). The crystals were air and water stable.

$K_2La_2Sb_2S_9$. This compound was synthesized from a mixture of 0.1103 g (1 mmol) K_2S, 0.0347 g (0.25 mmol) La, 0.0304 g (0.25 mmol) Sb, and 0.1283 g (4 mmol) S. The reagents were thoroughly mixed, sealed in an evacuated Pyrex ampoule, and heated at 400°C for 5 days (cooling 2°C/h). Pure yellow needles of $K_2La_2Sb_2S_9$ were obtained by isolation in degassed DMF and water (yield ~60% based on La metal). The crystals were air and water stable.

The elemental compositions of the materials were analyzed by scanning electron microscope/energy dispersive spectroscopy. Homogeneity for both compounds was confirmed by comparing the X-ray powder diffraction patterns of the products against those calculated using X-ray single-crystal data; see Tables 1 and 2.

TABLE 1
Calculated and Observed X-Ray Powder Pattern of $K_2Gd_2Sb_2Se_9$[a]

h	k	l	d_{calc} (Å)	d_{obs} (Å)	I/I_{max} (obs) (%)
1	1	0	9.630	9.576	13.6
0	2	0	8.831	8.781	100.0
1	2	0	7.001	6.953	80.9
2	0	0	5.744	5.705	35.6
2	1	0	5.462	5.427	29.4
1	3	0	5.239	5.203	6.9
0	4	0	4.415	4.383	32.5
2	3	0	4.111	4.088	14.7
0	2	1	3.808	3.783	9.9
3	1	0	3.742	3.717	21.3
3	2	0	3.513	3.485	49.3
1	3	1	3.287	3.264	17.8
3	3	0	3.210	3.186	19.8
0	4	1	3.051	3.030	54.1
1	4	1	2.949	2.928	52.3
3	4	0	2.893	2.872	10.6
4	1	0	2.835	2.815	43.1
4	2	0	2.731	2.711	70.4
2	4	1	2.694	2.677	17.7
4	3	0	2.581	2.563	20.2
1	7	0	2.464	2.448	9.5
4	4	0	2.408	2.390	16.9
4	1	1	2.353	2.341	22.3
2	7	0	2.310	2.293	13.4
4	2	1	2.293	2.277	13.7
3	5	1	2.211	2.196	14.4
4	3	1	2.202	2.188	20.1
1	8	0	2.168	2.153	57.5
0	0	2	2.110	2.095	14.2
2	8	0	2.061	2.046	24.1
3	6	1	2.042	2.028	14.6
5	2	1	1.967	1.954	8.8
0	8	1	1.956	1.943	6.5
5	5	0	1.926	1.912	15.5
3	8	0	1.912	1.899	8.2
6	1	0	1.904	1.890	12.0
2	9	0	1.857	1.844	17.6
5	4	1	1.835	1.823	5.9
3	2	2	1.809	1.798	7.4
0	10	0	1.766	1.753	11.2
4	8	0	1.750	1.737	16.7
4	2	2	1.669	1.659	5.0
4	3	2	1.634	1.623	3.6
4	4	2	1.587	1.578	4.1
7	4	0	1.538	1.528	6.8
1	8	2	1.512	1.502	5.5
7	2	1	1.507	1.498	4.9
2	8	2	1.474	1.462	8.1
2	11	1	1.452	1.443	3.8
6	7	1	1.434	1.424	8.3
5	5	2	1.423	1.414	5.4
2	9	2	1.394	1.385	4.5
0	10	2	1.354	1.347	5.2
4	8	2	1.347	1.340	5.5
7	8	1	1.257	1.249	5.7
4	12	1	1.251	1.243	5.6
9	3	0	1.248	1.240	5.6
3	6	3	1.205	1.198	4.1
10	0	1	1.109	1.101	3.9

[a] The *hkl* indices and the calculated *d* spacing are based on the substructure.

TABLE 2
Calculated and Observed X-Ray Powder Pattern of $K_2La_2Sb_2S_9$

h	k	l	d_{calc} (Å)	d_{obs} (Å)	I/I_{max} (obs) (%)
1	1	0	9.337	9.295	24.3
0	2	0	8.439	8.407	50.3
1	2	0	6.742	6.715	48.2
2	0	0	5.604	5.585	41.4
2	1	0	5.319	5.298	45.6
0	4	0	4.220	4.206	35.1
2	3	0	3.970	3.954	64.6
1	1	1	3.862	3.851	28.1
0	2	1	3.790	3.783	34.0
3	1	0	3.648	3.639	51.5
3	2	0	3.416	3.407	100.0
2	4	0	3.371	3.364	38.7
2	1	1	3.316	3.307	30.0
1	3	1	3.242	3.230	53.4
0	4	1	2.992	2.984	75.1
1	4	1	2.890	2.883	72.5
4	1	0	2.764	2.757	31.4
4	2	0	2.659	2.653	60.0
2	4	1	2.639	2.633	28.7
4	3	0	2.508	2.502	24.6
1	7	0	2.357	2.351	32.5
4	0	1	2.338	2.330	33.8
4	1	1	2.316	2.310	27.4
1	6	1	2.295	2.289	22.5
4	2	1	2.253	2.247	24.4
2	7	0	2.215	2.209	21.1
4	3	1	2.159	2.153	41.3
0	0	2	2.121	2.116	23.6
1	8	0	2.073	2.069	24.6
1	1	2	2.068	2.064	20.7
3	6	1	1.986	1.981	41.0
2	8	0	1.975	1.970	21.8
5	2	1	1.929	1.925	18.8
0	8	1	1.889	1.885	19.6
2	3	2	1.870	1.864	24.7
6	1	0	1.857	1.853	29.8
3	8	0	1.837	1.833	15.1
3	2	2	1.802	1.798	15.5
2	4	2	1.795	1.791	16.6
2	9	0	1.778	1.774	18.9
1	5	2	1.773	1.770	17.8
5	6	0	1.753	1.750	16.7
4	8	0	1.685	1.681	21.6
4	1	2	1.682	1.679	17.6
4	2	2	1.658	1.655	12.9
6	3	1	1.636	1.632	11.4
4	3	2	1.619	1.615	9.4
1	7	2	1.577	1.573	9.6
2	7	2	1.532	1.529	9.4
7	4	0	1.497	1.494	15.1
1	8	2	1.483	1.480	9.7
7	2	1	1.475	1.472	10.8
2	8	2	1.445	1.443	11.2
2	11	1	1.397	1.395	18.7
6	7	1	1.395	1.392	16.4
7	6	0	1.392	1.389	15.2
3	8	2	1.389	1.386	11.0
4	10	1	1.369	1.366	13.8
0	4	3	1.341	1.338	7.5
1	4	3	1.331	1.328	13.5
0	10	2	1.321	1.318	9.8
3	5	3	1.231	1.229	7.7
4	12	1	1.205	1.203	9.5
3	6	3	1.197	1.195	6.6
7	6	2	1.164	1.161	7.4
8	4	2	1.127	1.124	7.6

2.2. Physical Measurements

Solid state UV/Vis spectroscopy. Optical diffuse reflectance measurements were performed at room temperature with a Shimadzu UV-3101 PC double-beam, double-monochromator spectrophotometer operating in the 200–2500 nm region. The instrument is equipped with an integrating sphere and controlled by a personal computer. $BaSO_4$ was used as a 100% reflectance standard for all materials. Samples were prepared by grinding them to a fine powder, spreading them on a compacted surface of the powdered standard material, and preloading them into a sample holder. The reflectance versus wavelength data generated were used to estimate a material's band gap by converting reflectance to absorption data as described previously (12).

Magnetic susceptibility. The magnetic response of $K_2Gd_2Sb_2Se_9$ was measured over the range 2–300 K using a MPMS Quantum Design SQUID magnetometer. Sample was ground to a fine powder to minimize possible anisotropic effects and loaded into PVC containers. The temperature-dependent susceptibility studies were performed at 1000 G. Corrections for the diamagnetism of the sample containers were made by measuring the magnetic response of the empty container under the same conditions of temperature and field that were employed for the filled container. The diamagnetic contributions of all atoms to χ_m were taken into account according to Selwood (13).

Differential thermal analysis (DTA). DTA experiments were performed on a computer-controlled Shimadzu DTA-50 thermal analyzer. Typically a sample (~ 20 mg) of ground crystalline material was sealed in a silica ampoule under vacuum. A similar ampoule of equal mass filled with Al_2O_3 was sealed and placed on the reference side of the detector. The samples were heated to 800°C at 5°C/min and isothermed for 10 min followed by cooling at -5°C/min to 50°C. Residues of the DTA experiments were examined by X-ray powder diffraction. The stability and reproducibility of the samples were monitored by running multiple heating/cooling cycles.

Raman spectroscopy. Raman spectra were recorded on a Holoprobe Raman spectrograph equipped with a CCD camera detector using 633 nm radiation from a HeNe laser for excitation. Laser power at the sample was estimated to be about 5 mW and the focused laser beam diameter was ca. 10 μm. Five scans were needed to obtain good quality spectra. The accumulation time of each scan was 50 s.

2.3. X-Ray Crystallography

Substructure. Single crystals of $K_2Gd_2Sb_2Se_9$ with dimensions $0.13 \times 0.008 \times 0.008$ mm and $K_2La_2Sb_2S_9$ with dimensions $0.13 \times 0.003 \times 0.003$ mm were mounted on the tip of a glass fiber. Intensity data were collected at 293 K on a Siemens SMART Platform CCD diffractometer using graphite monochromatized Mo$K\alpha$ radiation over a hemisphere of reciprocal space. The individual frames were measured with an omega rotation of 0.3° and an acquisition time of 45 s per frame for $K_2Gd_2Sb_2Se_9$ and 60 s per frame for $K_2La_2Sb_2S_9$. SMART software (14) was used for data acquisition and SAINT (15) for data extraction and reduction. The absorption correction was done using SADABS (16). The complete data collection parameters and details of the structure solution and refinement for both compounds are given in Table 3.

Structure solution and refinement for both compounds were performed with the SHELXTL package of crystallographic programs (17). Systematic absence conditions of the data sets gave two possible space groups, *Pbam* and *Pba*2. The structure was solved and refined successfully in the *Pbam* space group. After successive refinements, the isotropic temperature factor for Sb(1) in $K_2Gd_2Sb_2Se_9$ was still very high ($U_{eq} = 0.04033$ Å^2 with $R1/wR2 = 0.1267/0.2478$ for all data) indicating that the Sb atoms may be positionally disordered in the structure. At a distance of 0.52 Å from Sb(1), a high electron density peak was found that behaved well as a disordered Sb and was assigned as Sb(2). For further refinement, the temperature factors, U_{ij}, for Sb(1) and Sb(2) were constrained to be equal and the sum of the occupancies of Sb(1) and Sb(2) was constrained to be the maximum allowed by the crystallgraphic site. After this procedure, temperature factors for Sb atoms and R indices dropped to reasonable values ($U_{eq} = 0.016$ Å^2 with $R1/wR2 = 0.0337/0.0424$ for all data). The Sb atoms appear to be disordered over Sb(1) and Sb(2) sites with 50% occupancy. The same Sb dirsorder model was adopted for the structure refinement of $K_2La_2Sb_2S_9$, which also showed a similar problematic behavior for Sb(1). The structure was successfully refined with reasonable isotropic temperature factors for the Sb atoms and R values. The temperature factors of the Se(5)/S(5) atoms were also high, probably due to the Sb atom disorder. The Se(5)/S(5) atoms are shared by four Sb atoms in the structure and, therefore, positional disorder of Sb atoms can cause positional fluctuation of the surrounding Se(5)/S(5) atoms. Judging from the abnormally high anisotropic temperature factor, U_{33}, of the Se(5)/S(5) atoms, the positions of the these atoms seemed to fluctuate mainly along the c axis. The other Se/S atoms are held not only by Sb atoms but also by the heavy and rigid Gd atoms, and their positions are not affected significantly by the Sb disorder. The coordinates of all atoms, isotropic temperature factors, and their estimated standard deviations (e.s.d.) are given in Table 4 and the anisotropic temperature factors are given in Table 5. Selected bond distance and angles are given in Tables 6 and 7.

TABLE 3
Summary of Crystallographic Data and Structure Analysis for $K_2Gd_2Sb_2Se_9$ and $K_2La_2Sb_2S_9$

	Formula		
	$K_2Gd_2Sb_2Se_9$	$K_2La_2Sb_2S_9$	$K_2Gd_2Sb_2Se_9$ (superstrucrture)
Formula weight	1346.84	888.06	1346.84
Crystal habit	Black needles	Yellow needles	Black needles
Space group	*Pbam*	*Pbam*	*C*2/*m*
a, Å	11.4880(3)	11.2080(5)	22.8783(4)
b, Å	17.6612(1)	16.8781(8)	8.4062(2)
c, Å	4.2201(1)	4.2419(2)	20.970(1)
Z; *V*, Å^3	2,856.22(3)	2,802.44(6)	8,3381.53(10)
D_{calc}, g/cm^3	5.224	3.675	5.291
Temp., K	293(2)	293(2)	171(2)
λ(Mo$K\alpha$), Å	0.71073	0.71073	0.71073
μ(Mo$K\alpha$), cm^{-1}	303.50	102.20	307.39
F(000)	1148	796	4592
θ_{max}, deg	28.13	24.98	28.30
Total data measured	5029	4896	15998
Unique data	1150	809	4306
	[$R_{int} = 0.040$]	[$R_{int} = 0.072$]	[$R_{int} = 0.071$]
No. of variables	51	51	162
Refinement method	Full-matrix least-squares on F^2		
Final R indices			
[$I > 2s$]	$R1^a = 0.0227$	$R1 = 0.0466$	$R1 = 0.0797$
	$wR2^b = 0.0403$	$wR2 = 0.0681$	$wR2 = 0.1689$
R indices (all data)	$R1 = 0.0337$	$R1 = 0.0649$	$R1 = 0.1141$
	$wR2 = 0.0424$	$wR2 = 0.0716$	$wR2 = 0.1782$
Goodness of fit on F^2	0.976	1.139	1.34

$^a R1 = \sum \| F_o | - | F_o \| / \sum | F_o |$.
$^b wR2 = \{\sum [w(F_o^2 - F_c^2)^2] / \sum [w(F_o^2)^2]\}^{1/2}$.

Superstructure of $K_2Gd_2Sb_2Se_9$. The positional disorder of the Sb atoms alerted us to the possibility of a superstructure in these materials. The existence of a superstructure for $K_2Gd_2Sb_2Se_9$ was probed by axial photographs on a Rigaku AFC6S diffractometer with a 4-h exposure time. The photographs showed weak superlattice peaks around every crystallographic axis resulting in a $2a \times 2b \times 2c$, eightfold supercell. Intensity data for the supercell were collected at 173.1 K on a Siemens SMART Platform CCD diffractometer using the same crystal used for the data collection

TABLE 4
Fractional Atomic Coordinates and Equivalent Atomic Displacement Parameter (U_{eq}) Values for $K_2Gd_2Sb_2Se_9$ (Substracture) and $K_2La_2Sb_2S_9$ with Estimated Standard Deviations in Parentheses

Atom	x	y	z	U_{eq}[a] (Å^2)
		$K_2Gd_2Sb_2Se_9$		
Gd	0.3838(1)	0.2030(1)	0.5	0.011(1)
Sb(1)[b]	0.0590(2)	0.1353(1)	0	0.016(1)
Sb(2)	0.0434(2)	0.1076(1)	0	0.016(1)
K	0.2166(2)	0.4435(1)	0.5	0.023(1)
Se(1)	0.3420(1)	0.3208(1)	0	0.013(1)
Se(2)	0.1180(1)	0.2203(1)	0.5	0.016(1)
Se(3)	0.0181(1)	0.3741(1)	0	0.018(1)
Se(4)	0.3160(1)	0.0903(1)	0	0.018(1)
Se(5)	0	0	0.5	0.032(1)
		$K_2La_2Sb_2S_9$		
La	0.3838(1)	0.2048(1)	0.5	0.013(1)
Sb(1)[b]	0.0616(5)	0.1338(3)	0	0.018(1)
Sb(2)	0.0439(5)	0.1052(3)	0	0.018(1)
K	0.2132(3)	0.4425(2)	0.5	0.025(1)
S(1)	0.3493(3)	0.3274(2)	0	0.017(1)
S(2)	0.1174(3)	0.2164(2)	0.5	0.034(1)
S(3)	0.0105(3)	0.3782(2)	0	0.023(1)
S(4)	0.3282(3)	0.0886(2)	0	0.022(1)
S(5)	0	0	0.5	0.077(3)

[a] U_{eq} is defined as one-third of the trace of the orthogonalized U_{ij} tensor.
[b] Sb(1) and Sb(2) are 50% occupied.

for the subcell with longer exposure time, 60 s per frame. The data were collected over a full sphere of reciprocal space, up to 28.30° in θ. The collected data were processed in the same way as described above. The complete data collection parameters and details of the structure solution and refinement for the superstructure for $K_2Gd_2Sb_2Se_9$ are given in Table 3. The preliminary cell given for the superstructure was orthorhombic with $a = 8.4294(2)$ Å, $b = 22.9352(2)$ Å, and $c = 35.2682(6)$ Å. As expected from the axial photographs, the unit cell is doubled along all three axes resulting in an eight-fold supercell. Each cell parameter of the supercell is slightly smaller than each subcell parameter multiplied by two because intensity data for the supercell were collected at a lower temperature. The systematic absence conditions suggested three possible space groups: *Fmmm*, *Fmm*2, and *F*222; none of which, however, turned out to be satisfactory. It was suspected that the crystal system of the supercell might no longer be orthorhombic. If the subtle structural change, which gives rise to the supercell, deprives the crystal of any of the three diads (rotation and/or inversion), then the crystal system must be lowered in symmetry even though the α, β, and γ angles remain 90°.

From the substructure, it was possible to deduce the space group of the supercell by considering the result of doubling all the cell parameters. The screw axes or glide planes found in the substructure might be lost in the superstructure because their symmetry operation includes a fractional translation along the axes. The subcell that has the space group $P2_1/b2_1/a2/m$ has four translational symmetry elements; two 2_1 screw axes along the *a* and *b* directions: a *b* glide plane perpendicular to the *a* axis and an *a*-glide plane perpendicular to the *b* axis. In this case, doubling of all three cell parameters eliminates all screw axes and glide planes present in the substructure. Only two-fold axes paralel to the *c* direction and mirror planes perpendicular to the same axis remain. The loss of both screw axes and glide planes forces the crystal system to be lowered to monoclinic.

It is obvious that the *c* axis, which still has two-fold axes parallel to it as well as perpendicular mirror planes, must be the unique *b*′ axis for the monoclinic setting of the superstructure. As mentioned previously, systematic absence conditions (*hkl*: $h + k = 2n$, $h + 1 = 2n$, $k + 1 = 2n$) indicate that the supercell has *F* centering. Monoclinic *F* can be transformed to monoclinic *C* by reducing the cell volume by half; see Scheme 1. Consequently, the superstructure has a *C* centered monoclinic cell and the unique axis b′ could have a parallel two-fold axis and/or a perpendicular mirror plane depending on the arrangement of atoms in the supercell. Therefore, the space group should be either *C*2/*m*, *Cm*, or *C*2. The vectorial relationships between the supercell

TABLE 5
Anisotropic Displacement Parameters (Å^2×10^3) for $K_2Gd_2Sb_2Se_9$ (Substructure) and $K_2La_2Sb_2S_9$

	U_{11}	U_{22}	U_{33}	U_{23}	U_{13}	U_{12}
			$K_2Gd_2Sb_2Se_9$			
Gd	14(1)	10(1)	9(1)	0	0	0(1)
Sb(1)	17(1)	15(1)	17(1)	0	0	0(1)
Sb(2)	17(1)	15(1)	17(1)	0	0	0(1)
K	28(1)	21(1)	19(1)	0	0	0(1)
Se(1)	16(1)	12(1)	13(1)	0	0	1(1)
Se(2)	13(1)	16(1)	20(1)	0	0	2(1)
Se(3)	18(1)	21(1)	14(1)	0	0	− 5(1)
Se(4)	22(1)	15(1)	16(1)	0	0	− 2(1)
Se(5)	26(1)	12(1)	56(1)	0	0	− 1(1)
			$K_2La_2Sb_2S_9$			
La	12(1)	16(1)	9(1)	0	0	0(1)
Sb(1)	16(2)	23(2)	14(1)	0	0	3(2)
Sb(2)	16(2)	23(2)	14(1)	0	0	3(2)
K	25(2)	28(2)	22(2)	0	0	1(1)
S(1)	18(2)	20(2)	13(2)	0	0	2(1)
S(2)	13(2)	25(2)	63(3)	0	0	0(2)
S(3)	22(2)	33(2)	14(2)	0	0	− 11(2)
S(4)	26(2)	19(2)	20(2)	0	0	− 3(2)
S(5)	30(4)	16(3)	184(10)	0	0	2(3)

Note. U_{ij} for Sb(1) and Sb(2) are constrained to be equal.

TABLE 6
Selected Distances (Å) and Bond Angles (°) for $K_2Gd_2Sb_2Se_9$ (Substructure)

	Bond distances		
Gd–Se(1)	3.0010(5) × 2	Sb(1)–Se(1)	2.611(3)
Gd–Se(2)	3.0123(7)	Sb(1)–Se(2)	2.6763(14) × 2
Gd–Se(2)	3.0685(7)	Sb(1)–Se(4)	3.058(3)
Gd–Se(3)	2.9478(5) × 2	Sb(1)–Se(5)	3.260(2) × 2
Gd–Se(4)	3.0044(6) × 2	Sb(2)–Se(1)	2.638(2)
Sb(1)–Sb(2)	0.522(2)	Sb(2)–Se(2)	3.024(2) × 2
Se(3)–Se(4)	2.4055(10)	Sb(2)–Se(4)	3.146(2)
		Sb(2)–Se(5)	2.8830(14) × 2
	Bond angles		
Se(1)–Gd–Se(1)	89.35(2)	Se(1)–Sb(1)–Se(2)	94.32(6)
Se(1)–Gd–Se(2)	76.82(2)	Se(1)–Sb(1)–Se(4)	177.82(9)
Se(1)–Gd–Se(2)	80.30(2)	Se(1)–Sb(1)–Se(5)	91.10(6)
Se(1)–Gd–Se(3)	84.30(2)	Se(2)–Sb(1)–Se(2)	104.08(8)
Se(1)–Gd–Se(3)	155.13(2)	Se(2)–Sb(1)–Se(4)	95.0(5)
Se(1)–Gd–Se(4)	85.63(2)	Se(2)–Sb(1)–Se(5)	40.53(5)
Se(1)–Gd–Se(4)	155.74(2)	Se(2)–Sb(1)–Se(5)	87.33(2)
Se(2)–Gd–Se(2)	147.586(13)	Se(2)–Sb(1)–Se(5)	166.93(7)
Se(2)–Gd–Se(3)	124.52(2)	Se(4)–Sb(1)–Se(5)	90.56(5)
Se(2)–Gd–Se(3)	74.94(2)	Se(5)–Sb(1)–Se(5)	80.68(5)
Se(2)–Gd–Se(4)	78.93(2)	Se(1)–Sb(2)–Se(2)	86.15(6)
Se(2)–Gd–Se(4)	121.98(2)	Se(1)–Sb(2)–Se(4)	156.92(8)
Se(3)–Gd–Se(3)	91.42(2)	Se(1)–Sb(2)–Se(5)	99.46(6)
Se(3)–Gd–Se(4)	47.66(2)	Se(2)–Sb(2)–Se(2)	88.48(6)
Se(3)–Gd–Se(4)	109.39(2)	Se(2)–Sb(2)–Se(4)	77.42(5)
Se(4)–Gd–Se(4)	89.23(2)	Se(2)–Sb(2)–Se(5)	88.402(11)
		Se(2)–Sb(2)–Se(5)	173.38(9)
		Se(4)–Sb(2)–Se(5)	96.20(6)
		Se(5)–Sb(2)–Se(5)	94.09(6)

parameters, a', b', c', and the subcell parameters, a, b, c, are as follows:

$$a' = -2a, \quad b' = 2c, \quad c' = a + b$$

The superstructure was solved and refined successfully in the space group $C2/m$ confirming that, from all the symmetry elements present in the *Pbam* symmetry of the subcell, only the two-fold axes that are parallel to the c axis and the mirror planes perpendicular to the c axis ($= b'$ axis) are valid. No Sb atom disorder was evident in the eight-fold superstructure of $K_2Gd_2Sb_2Se_9$. The apparent Sb atom disorder in the substructure, therefore, is an artifact. The coordinates of all atoms, isotropic temperature factors, and their estimated standard deviations are given in Table 8.

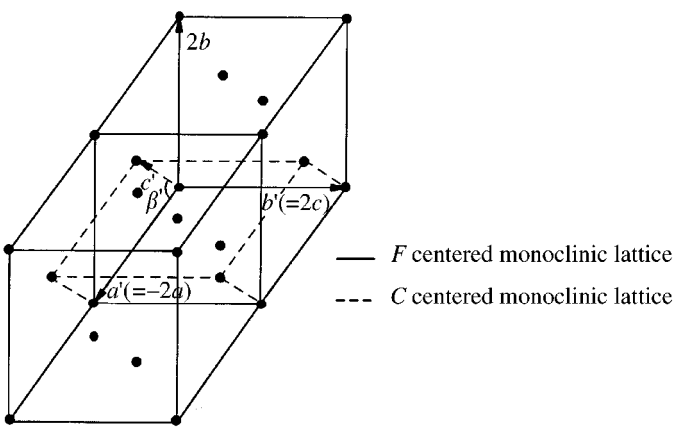

SCHEME 1

3. RESULTS AND DISCUSSION

3.1. Substructure

Since both $K_2Gd_2Sb_2Se_9$ and $K_2La_2Sb_2S_9$ have the same structure, only the former will be discussed in detail. $K_2Gd_2Sb_2Se_9$ has a three-dimensional tunnel framework with Gd^{3+} centers (Fig. 1). The coordination geometry around the Gd^{3+} atom is a bicapped trigonal prism of Se atoms (Fig. 2a). There are four Se^{2-} ions sitting at two apices and two capping sites of the prism. The other four Se atoms are from two diselenide groups that form the two short parallel edges of the trigonal prism. The Se–Se distance is normal at 2.405(1) Å (2.118(6) Å for S–S bond in $K_2La_2Sb_2S_9$). The formula of the compounds can be described as $K_2^+Gd_2^{3+}Sb_2^{3+}(Se^{2-})_5(Se_2)_2^{2-}$. The Gd^{3+}

TABLE 7
Selected Distances (Å) and Bond Angles (°) for $K_2La_2Sb_2S_9$

	Bond distances		
La–S(1)	2.988(3) × 2	Sb(1)–S(1)	2.469(7)
La–S(2)	2.936(4)	Sb(1)–S(2)	2.614(4) × 2
La–S(2)	2.992(4)	Sb(1)–S(4)	3.084(7)
La–S(3)	2.912(2) × 2	Sb(1)–S(5)	3.174(4) × 2
La–S(4)	2.955(2) × 2	Sb(2)–S(1)	2.460(6)
Sb(1)–Sb(2)	0.522(5)	Sb(2)–S(2)	2.949(4) × 2
S(3)–S(4)	2.118(5)	Sb(2)–S(4)	3.199(7)
		Sb(2)–S(5)	2.810(3) × 2
	Bond angles		
S(1)–La–S(1)	90.45(10)	S(1)–Sb(1)–S(2)	95.1(2)
S(1)–La–S(2)	78.58(8)	S(1)–Sb(1)–S(4)	178.9(2)
S(1)–La–S(2)	79.95(8)	S(1)–Sb(1)–S(5)	88.79(14)
S(1)–La–S(3)	83.07(8)	S(2)–Sb(1)–S(2)	108.5(2)
S(1)–La–S(3)	155.99(10)	S(2)–Sb(1)–S(4)	84.3(2)
S(1)–La–S(4)	85.57(7)	S(2)–Sb(1)–S(5)	42.20(14)
S(1)–La–S(4)	160.34(9)	S(2)–Sb(1)–S(5)	83.65(7)
S(2)–La–S(2)	149.34(4)	S(2)–Sb(1)–S(5)	166.8(2)
S(2)–La–S(3)	121.20(8)	S(4)–Sb(1)–S(5)	92.0(2)
S(2)–La–S(3)	77.47(9)	S(5)–Sb(1)–S(5)	83.85(12)
S(2)–La–S(4)	80.39(8)	S(1)–Sb(2)–S(2)	87.3(2)
S(2)–La–S(4)	119.23(8)	S(1)–Sb(2)–S(4)	157.5(2)
S(3)–La–S(3)	93.50(10)	S(1)–Sb(2)–S(5)	97.86(14)
S(3)–La–S(4)	42.31(10)	S(2)–Sb(2)–S(2)	92.0(2)
S(3)–La–S(4)	107.82(9)	S(2)–Sb(2)–S(4)	77.15(14)
S(4)–La–S(4)	91.73(10)	S(2)–Sb(2)–S(5)	84.74(5)
		S(2)–Sb(2)–S(5)	173.7(2)
		S(4)–Sb(2)–S(5)	96.85(14)
		S(5)–Sb(2)–S(5)	98.0(2)

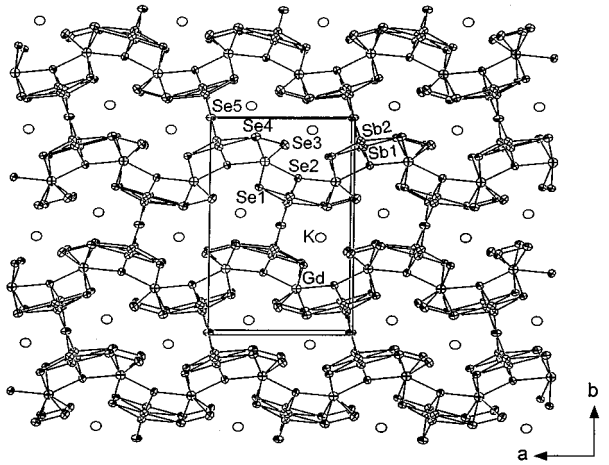

FIG. 1. ORTEP representation of $K_2Gd_2Sb_2Se_9$ viewed down the *c* axis with labeling (90% probability ellipsoids). The labeling scheme for the $K_2La_2Sb_2S_9$ is analogous.

centered trigonal prism is sharing its triangular faces with neighboring prisms along the *c* axis forming one-dimensional columns similar to those found in $ZrSe_3$ (18). The columns are arranged side by side and connected by sharing Se atoms on the capping sites of the trigonal prisms forming sheets (Fig. 2b). The difference with $ZrSe_3$ lies in the connectivity of single columns to build layers. In $ZrSe_3$, each trigonal prismatic column shares Se atoms at the apex and capping sites with neighboring columns, so that the apices in one become caps in the next. In contrast to $ZrSe_3$, $K_2Gd_2Sb_2Se_9$ has columns that share Se atoms only at the capping sites (Fig. 2c). As a result, each layer of $ZrSe_3$ is built from bilayers of Zr atoms while each layer of $K_2Gd_2Sb_2Se_9$ consists of only monolayers of Gd atoms.

The antimony atoms in the compounds have a formal charge of $+3$. These atoms appear to be positionally disordered over two crystallographically different sites, Sb(1) and Sb(2), with 50% occupancy. The distance between the two sites is 0.522(2) Å. The Sb^{3+} ions are stabilized in distorted octahedral sites (Fig. 3a). The local symmetry of the Sb^{3+} ion can be described as intermediate between trigonal pyramidal and octahedral with three shorter Sb–Se bonds ranging from 2.618 to 2.883 Å and three longer Sb–Se bonds ranging from 3.024 to 3.260 Å. This type of distorted environment indicates that the 5*s* lone pair of Sb is stereochemically expressing itself and it is directed toward the three longer Sb–Se bonds. Both Sb(1) and Sb(2) sites are located inside of the same octahedral pocket and have the same type of distortion. For example, Sb1 is making three shorter bonds with Se(1), Se(2), and Se(2′) and three longer bonds with Se(5), Se(5′), and Se(4) while Sb(2) is making

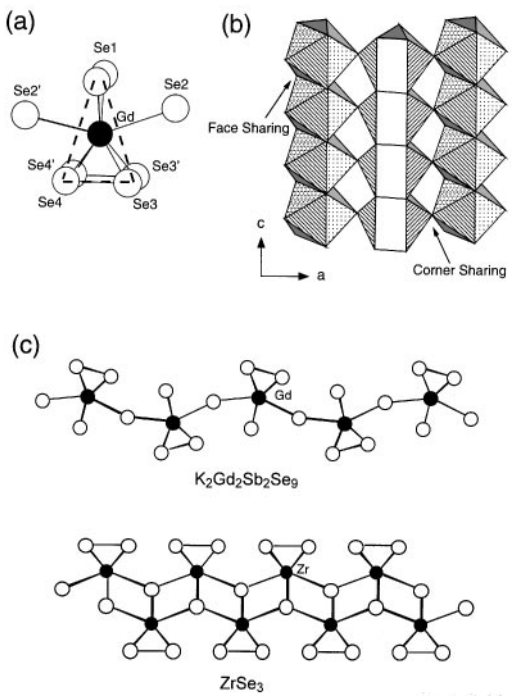

FIG. 2. (a) Coordination environment of the Gd atom. (b) Polyhedral representation of the Gd^{3+}-centered bicapped trigonal prisms. The prisms share corners along the *a* axis and triangular faces along the *c* axis to form layers. (c) Comparison of the layers of $K_2Gd_2Sb_2Se_9$ and $ZrSe_3$.

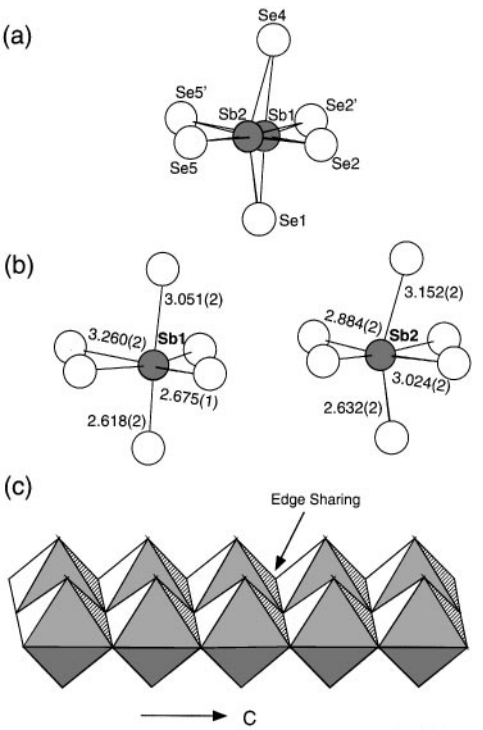

FIG. 3. (a) Coordination environment of the Sb atoms. (b) Distortion in the $Sb(1)Se_6$ and $Sb(2)Se_6$ octahedra. (c) Polyhedral representation of the $SbSe_6$ octahedral blocks along the *c* axis.

three shorter bonds with Se(1), Se(5), and Se(5′) and three longer bonds with Se(2), Se(2′), and Se(4) (Fig. 3b). In $K_2La_2Sb_2S_9$, the Sb^{3+} ion is also disordered in the same manner as in $K_2Gd_2Sb_2Se_9$, but the geometry around Sb is much more distorted than that in the case of $K_2Gd_2Sb_2Se_9$ (Table 7). The $SbSe_6$ octahedra share edges with neighboring $SbSe_6$ octahedra forming an infinite chain along the *c* axis (Fig. 3c). Two such single chains also share edges making infinite double chains of Sb atoms, which then bridge Gd layers together to make the whole framework three-dimensional.

The K^+ filled tunnels run parallel to the *c* axis. The K^+ ions are coordinated by seven selenium atoms in monocapped trigonal prismatic sites with an average (K–Se) distance of 3.36 Å ((K–S) distance of 3.29 Å for $K_2La_2Sb_2S_9$).

3.2. *Superstructure of $K_2Gd_2Sb_2Se_9$*

In the superstructure, Sb atoms are fully ordered occupying Sb(1) and Sb(2) sites alternatively with full occupancy instead of statistical disorder over the two sites. The overall superstructure view down the *b*′ axis is shown in Fig. 4(a). The unit cell of the subcell is also shown with a dotted line for comparison. The labeling scheme for the atoms in the supercell are devised to preserve the numbering of the Sb and Se atoms in the subcell for the sake of comparison. For example, Se(1a), Se(1b), Se(1c), and Se(1d) in the supercell are derived from the same atom, Se(1), in the subcell. Figure 4b shows space-group diagrams of *Pbam* and *C*2/*m* view down the *c* and *b*′ axes, respectively. As explained previously, the *a* and *b* glide planes and the 2_1 screw axes present in *Pbam* no longer exist in *C*2/*m*. Instead, an *a*-glide plane perpendicular to the *b*′ axis and *a* 2_1 axis parallel to the *b*′ axis are generated by the positional ordering of the Sb atoms in the superstructure.

The arrangement of Sb atoms in the Sb double chain along the *b*′ axis in the superstructure is shown in Fig. 5 compared with that in the substructure. Figures 5a and 5b are ball and stick representations of edge-sharing Sb octahedra that were shown previously as a polyhedral representation in Fig. 3c. The axial Se atoms that do not have any structural variations are omitted for clarity. The two rows of Sb atoms sandwich a row of Se(5*a*) atoms. Each Sb row is composed of Sb(1*a*) and Sb(2*a*) sitting alternatively. This is how the unit cell is doubled along the $c(=b')$ axis. Since Sb(1*a*) is making longer bonds with Se(5*a*), and Sb(2*a*) is making shorter bonds with Se(5*a*), the Sb atom propagation along the *b*′ axis is not a straight line but rather zigzags. In the substructure, the coordination environment of Se(5) seemed to be square planar. However, the ordering of the Sb

TABLE 8
Fractional Atomic Coordinates and Equivalent Atomic Displacement Parameter (U_{eq}) Values for $K_2Gd_2Sb_2Se_9$ (Superstructure)

Atom	*x*	*y*	*z*	U_{eq}[a] (Å^2)
Gd(1)	0.2934(1)	0.2505(2)	0.2030(1)	0.011(1)
Gd(2)	0.0903(1)	0.2483(2)	0.2970(1)	0.011(1)
Sb(1a)	0.4608(1)	0.5	0.3648(1)	0.013(1)
Sb(1b)	0.0967(2)	0	0.1318(2)	0.026(1)
Sb(2a)	0.4687(1)	0	0.3930(1)	0.014(1)
Sb(2b)	0.0760(2)	0.5	0.1106(2)	0.031(1)
K(1)	0.8866(3)	0.2529(9)	0.0564(3)	0.023(1)
K(2)	0.3300(3)	0.2487(9)	0.4436(4)	0.025(1)
Se(1a)	0.3292(2)	0.5	0.3187(2)	0.014(1)
Se(1b)	0.0089(2)	0.5	0.1783(2)	0.015(1)
Se(1c)	0.3334(2)	0	0.3227(2)	0.012(1)
Se(1d)	0.0121(2)	0	0.1797(2)	0.012(1)
Se(2a)	−0.0513(1)	0.2415(4)	0.2794(2)	0.015(1)
Se(2b)	0.1694(1)	0.2428(4)	0.2206(2)	0.016(1)
Se(3a)	0.3194(2)	0.5	0.1242(3)	0.020(1)
Se(3b)	0.6112(2)	0	0.4067(2)	0.015(1)
Se(3c)	0.3248(2)	0	0.1277(2)	0.014(1)
Se(3d)	0.1955(2)	0	0.3753(2)	0.017(1)
Se(4a)	0.2010(2)	0.5	0.0901(2)	0.018(1)
Se(4b)	0.1965(2)	0.5	0.3729(2)	0.019(1)
Se(4c)	0.2054(2)	0	0.0903(2)	0.018(1)
Se(4d)	0.6142(2)	0.5	0.4128(2)	0.017(1)
Se(5a)	0.5	0.2283(5)	0.5	0.019(1)
Se(5b)	0	0.2689(6)	0	0.023(1)

[a] U_{eq} is defined as one-third of the trace of the orthogonalized U_{ij} tensor.

TABLE 9
Selected Distances (Å) and Bond Angles (°) for $K_2Gd_2Sb_2Se_9$ (superstructure)

Bond distances			
Gd(1)–Se(1a)	2.965(3) × 2	Gd(2)–Se(1b)	3.014(3)
Gd(1)–Se(1c)	3.011(3)	Gd(2)–Se(1d)	2.968(3)
Gd(1)–Se(2b)	3.055(3)	Gd(2)–Se(2a)	3.056(3)
Gd(1)–Se(3a)	2.925(3)	Gd(2)–Se(2b)	3.000(3) × 2
Gd(1)–Se(3c)	2.946(3)	Gd(2)–Se(3b)	2.967(3)
Gd(1)–Se(4a)	3.003(3)	Gd(2)–Se(4b)	2.949(3)
Gd(1)–Se(4c)	2.981(3)	Gd(2)–Se(4d)	3.019(3)
Sb(1a)–Se(1a)	2.617(5)	Sb(2a)–Se(1c)	2.605(4)
Sb(1a)–Se(2a)	2.609(3) × 2	Sb(2a)–Se(2a)	3.068(3) × 2
Sb(1a)–Se(4d)	3.074(5)	Sb(2a)–Se(3b)	3.113(5)
Sb(1a)–Se(5a)	3.372(3) × 2	Sb(2a)–Se(5a)	2.735(4) × 2
Sb(1b)–Se(1b)	2.599(5)	Sb(2b)–Se(1d)	2.619(5)
Sb(1b)–Se(2b)	3.031(4) × 2	Sb(2b)–Se(2b)	2.650(4) × 2
Sb(1b)–Se(4a)	3.114(5)	Sb(2b)–Se(4c)	3.051(5)
Sb(1b)–Se(5b)	2.790(4) × 2	Sb(2b)–Se(5b)	3.313(4) × 2
K(1)–Se(1b)	3.298(7)	K(2)–Se(1a)	3.357(8)
K(1)–Se(1d)	3.371(7)	K(2)–Se(1c)	3.319(8)
K(1)–Se(3a)	3.359(8)	K(2)–Se(3b)	3.380(7)
K(1)–Se(3c)	3.294(7)	K(2)–Se(3d)	2.382(6)
K(1)–Se(4a)	3.326(7)	K(2)–Se(4b)	3.325(7)
K(1)–Se(4c)	3.371(7)	K(2)–Se(4d)	3.312(8)
K(1)–Se(5b)	3.391(6)	K(2)–Se(5a)	3.397(6)
Se(3a)–Se(4a)	2.395(6)	Se(3c)–Se(4c)	2.396(6)
Se(3b)–Se(4b)	2.413(6)	Se(3d)–Se(4d)	2.382(6)

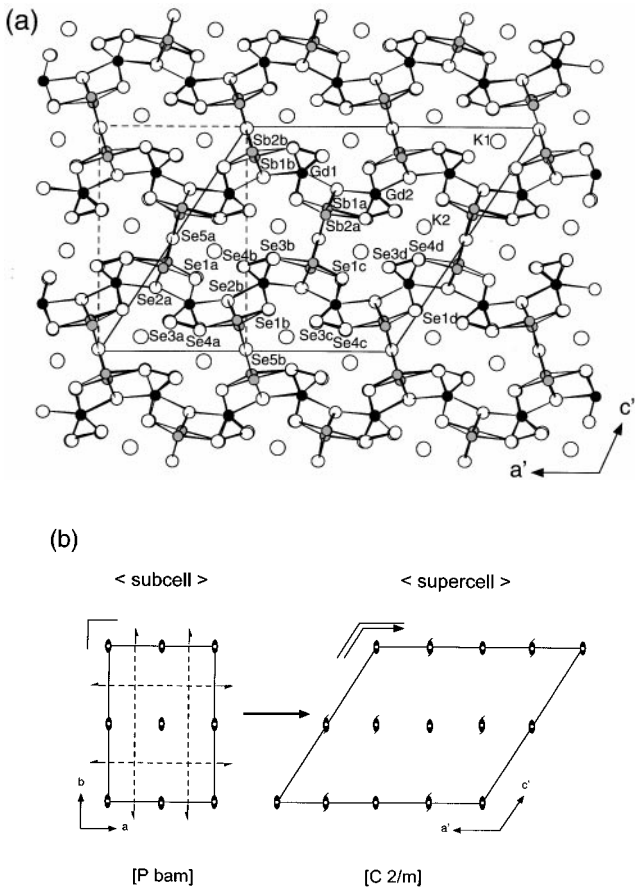

FIG. 4. (a) The superstructure of $K_2Gd_2Sb_2Se_9$ viewed down the b' axis with labeling. The solid line represents the unit cell for the superstructure and the dotted line represents the unit cell for the substructure. (b) Corresponding space group diagrams for *Pbam* and *C*2/*m* view down the c and b' axes, respectively.

atoms in the superstructure reduces the square planar symmetry and causes the Se(5) atoms to have two short bonds with Sb(2*a*) and two long bonds with Sb(1*a*).

The unit cell is doubled along the a and b direction because of the way that the Sb chains are arranged with respect to one another in the space. Every other Sb chain along the a and the b axis is shifted by $1/2c$ ($= 1/4b'$), which is the distance between Sb(1) and Sb(2) in the Sb chain, so that Sb(1) in one chain and Sb(2) in the next chain can sit on the same ab plane causing the repeating unit along the a and the b axes to double.

The zigzag arrangement of the Sb atoms, which causes the eight fold superstructure, can be interpreted as a result of the ordering of the 5*s* lone pairs of Sb ions. Figure 5c shows two different orientations of the lone pairs of Sb(1*a*) and Sb(2*a*) ions. The lone pairs of Sb(1*a*) are directed toward Se(5*a*) atoms and those of Sb(2*a*) are directed toward Se(2*a*) atoms.

Figure 5b also shows that the positions of Se(5*a*) atoms in the superstructure are modulated along the b' axis. As a result, there are two different Se(5*a*)–Se(5*a*) distances in the superstructure; one is short and the other is long, while all the Se(5)–Se(5) distances are all equal in the substructure. This explains why the temperature factor for Se(5) is high in the substructure refinement and why only the U_{33} component for Se(5), which represents the positional displacement along the c axis ($= b'$ axis), has a high value. Since the superstructure allows this modulation of Se(5) atoms, the temperature factors of Se(5*a*) and Se(5*b*), which is derived from Se(5) in the subcell, now have reasonable values.

The positional variation of Gd, K, and Se atoms (except for Se(5)) in the superstructure are negligible with respect to those in the substructure. The supercell is, therefore, entirely attributed to the Sb positional ordering caused by the steric requirements of the $5s^2$ lone pair.

We believe that the same kind of superstructure exists in $K_2La_2Sb_2S_9$ judging from the same problematic behavior

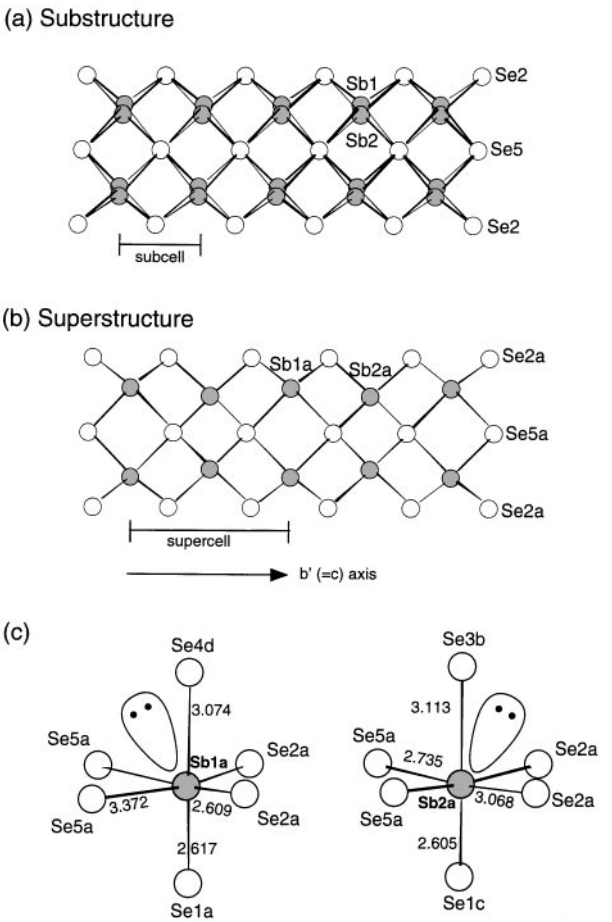

FIG. 5. Ball and stick representation of the edge-shared $SbSe_6$ octahedra along the b' axis ($= c$ axis) for (a) the substructure and (b) the superstructure.

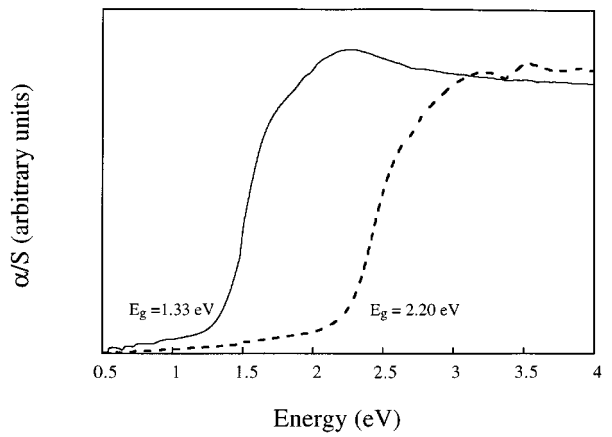

FIG. 6. Optical absorption spectra of $K_2Gd_2Sb_2Se_9$ (—) and $K_2La_2Sb_2S_9$ (. . .). The band gap value, E_g, is shown.

of Sb and S(5) atoms in the subcell. Since sulfur atoms are lighter than selenium atoms, positional variations for the other S atoms as well as that of S5 atoms in the superstructure are expected to be more significant than those of Se atoms in $K_2Gd_2Sb_2Se_9$. Nevertheless, attempts to refine the superstructure of $K_2La_2Sb_2S_9$ were unsuccessful due to the small crystal dimensions and insufficient diffraction quality.

3.3. *Properties*

The compounds reported here are valence precise and are expected to be semiconductors. The absorption spectra confirm this by showing the presence of abrupt optical gaps (Fig. 6). The band gaps of $K_2Gd_2Sb_2Se_9$ and $K_2La_2Sb_2S_9$ occur at 1.33 and 2.20 eV, respectively. DTA experiments showed that $K_2Gd_2Sb_2Se_9$ melts congruently at 597°C. $K_2La_2Sb_2Se_9$ decomposed gradually above 400°C perhaps because of a reaction with the container.

Magnetic susceptibility measurements of $K_2Gd_2Sb_2Se_9$ as a function of temperature show Curie–Weiss behavior between 4 and 300 K with $\theta = -5.3$ K (Fig. 7). The μ_{eff} calculated from the slope of the straight line is 7.96 B.M., which is in good agreement with the theoretical μ_{eff} value of a free ion Gd^{3+} (7.94 B.M.) with f^7 configuration (19).

The Raman spectra of $K_2Gd_2Sb_2Se_9$ and $K_2La_2Sb_2S_9$ are shown in Fig. 8. The shifts at 266 cm^{-1} for $K_2Gd_2Sb_2Se_9$ and 473 cm^{-1} for $K_2La_2Sb_2S_9$ are assigned to the stretching vibration of the dichalcogenide groups and these values are in accord with the Se–Se/S–S stretching frequencies reported for other compounds (11, 20, 21). The strong shift at 218 cm^{-1} in Fig. 8a is attributed to a Sb–Se vibration, which causes an overtone at 445 cm^{-1}.

4. CONCLUSION

Polychalcoantimonate fluxes were used for the synthesis of new quaternary compounds, $K_2Gd_2Sb_2Se_9$ and $K_2La_2Sb_2S_9$, which adopt a new structure type. These

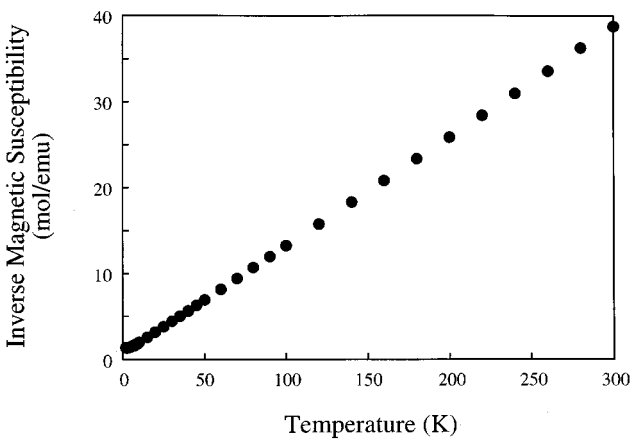

FIG. 7. Inverse molar magnetic susceptibility, $1/\chi_m$ (based on Gd metal), of $K_2Gd_2Sb_2Se_9$ versus temperature.

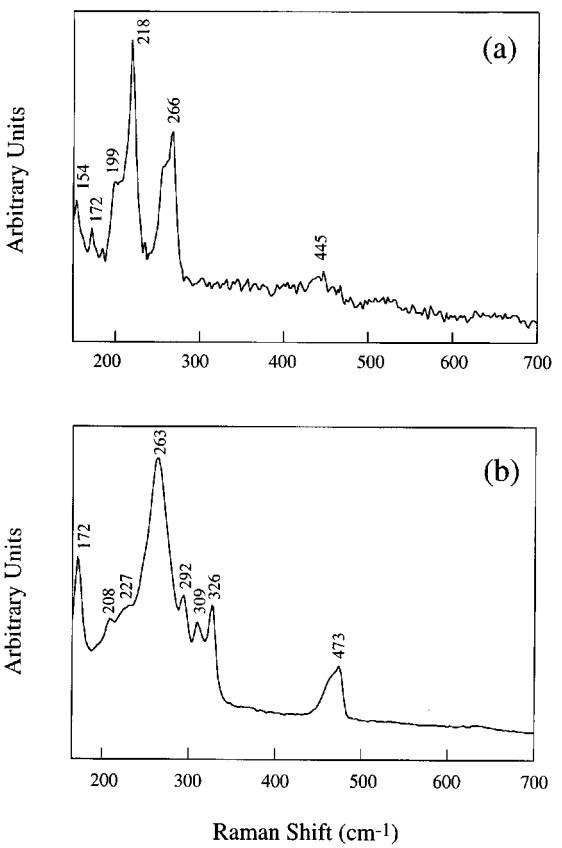

FIG. 8. Raman spectra of (a) $K_2Gd_2Sb_2Se_9$ and (b) $K_2La_2Sb_2S_9$.

compounds are a good example of how the $5s^2$ lone pair of the Sb^{3+} ion can induce a novel and elaborate framework by distorting its local environment. To reduce steric repulsion between the lone pairs of adjacent Sb ions in the edge-shared octahedral blocks, the ions adopt a zigzag arrangement, which results in a $2a \times 2b \times 2c$ superstructure. This structure type seems to be quite stable and easily formed with other lanthanide metals. We have already prepared many more members of $K_2Ln_2Sb_2Se_9$ family (A = K, Rb; Ln = Sm, Ce, Tb, and Dy) with the same reaction conditions (22). Only the reactions with Eu metal, which prefers $+2$ oxidation state, produced compounds with a different structure (23).

ACKNOWLEDGMENTS

Financial support from the Office of Naval Research (Contract N00014-98-1-0443) is gratefully acknowledged. The authors are grateful to the X-ray Crystallogrphic Laboratory of the University of Minnesota and to Dr. Victor G. Young, Jr., for collecting the single crystal X-ray data sets for $K_2La_2Sb_2S_9$. This work made use of the W. M. Keck Microfabrication Facility at MSU, a NSF MRSEC facility. The Siemens SMART platform CCD diffractometer was purchased with funds from the National Science foundation (CHE-9634638). This work made use of the SEM facilities of the Center for Electron Optics at Michigan State University.

REFERENCES

1. M. G. Kanatzidis, *Curr. Opin. Solid State Mater. Sci.* **2,** 139 (1997).
2. K.-S. Choi, L. Iordanidis, K. Chondroudis, and M. G. Kanatzidis, *Inorg. Chem.* **36,** 3804 (1997).
3. D.-Y. Chung, K.-S. Choi, L. Iordanidis, J. L. Schindler, P. Brazis, C. R. Kannewurf, B. Chen, S. Hu, C. Uher, and M. G. Kanatzidis, *Chem. Mater.* **9,** 3060 (1997).
4. (a) J. A. Hanko, Ph.D. dissertation, Michigan State University, 1998; (b) P. T. Wood, G. L. Schimek, and J. W. Kolis, *Chem. Mater.* **8,** 721 (1996); (c) G. L. Schimek, T. L. Pennington, P. T. Wood, and J. W. Kolis, *J. Solid State Chem.* **123,** 277 (1996).
5. J. A. Hanko and M. G. Kanatzidis, *J. Chem. Soc. Chem. Commun.* 725 (1998).
6. J. A. Hanko and M. G. Kanatzidis, *J. Alloys Compd.* **280,** 71 (1998).
7. J. A. Hanko and M. G. Kanatzidis, manuscript in preparation.
8. M. Imafuku, I. Nakai, and K. Nagashima, *Mater. Res. Bull.* **21,** 493 (1986).
9. J. Li, Z. Chen, X. Wang, and D. M. Proserpio, *J. Alloys Compd.* **262–263,** 28 (1997).
10. J. H. Chen and P. K. Dorhout, *J. Alloys Compd.* **249,** 199 (1997).
11. K.-S. Choi and M. G. Kanatzidis, submitted for publication.
12. T. J. McCarthy, S.-P. Ngeyi, J.-H. Liao, D. Degroot, T. Hogan, C. R. Kannewurf, and M. G. Kanatzidis, *Chem. Mater*, **5,** 331 (1993).
13. P. W. Selwood, *in* "Magnetochemistry," 2nd ed. Interscience, New York, 1956.
14. SMART: Siemens Analytical X-ray Systems, Inc., Madison WI 53719, 1994.
15. SAINT: Version 4, Seimens Analytical X-ray Systems. Inc., Madison, WI53719, 1994–1996.
16. G. M. Sheldrick, University of Göttingen, Germany, to be published.
17. SHELXTL: Version 5, G. M. Sheldrick, Siemens Analytical X-ray Systems, Inc., Madison, WI 53719, 1994.
18. Von W. Krönert and K. Plieth, *Z. Anorg. Allg. Chem.* **336,** 207 (1965).
19. R. S. Drago, *in* "Physical Methods for Chemists," 2nd ed. Saunders College Publishing, New York, 1992.
20. P. Böttcher and J. Getzschmann, R. Keller, Z. *Anorg. Allg. Chem.* **619,** 476 (1993).
21. K.-S. Choi, R. R. Patschke, S. J. L. Billinge, M. J. Waner, M. Dantus, and M. G. Kanatzidis, *J. Amer. Chem. Soc.* **120,** 10706 (1998).
22. K.-S. Choi and M. G. Kanatzidis, unpublished work.
23. K.-S. Choi and M. G. Kanatzidis, manuscript in preparation.